Tuijin Jishu/Journal of Propulsion Technology
ISSN: 1001-4055
Vol. 44 No. 4 (2023)

Investigation of Ionospheric Disturbance in ALOS PALSAR Images Using Machine Learning

Manaswini R [1] , G Raju[2]

[1] *Research scholar, Dept of ECE Jain Deemed-to-be University kanakapura road, Jakkasandra, post Bengaluru, Karnataka 562112, India. And Assistant Professor Dept of ECE, School of Engineering Technology Presidency University Itigalpura Rajanakunte Yelahanka Bangalore 560064.*

[2] *Professor, Dept of ECE Jain Deemed-to-be University kanakapura road, Jakkasandra, post-Bengaluru, Karnataka 562112, India*

Abstract.: The ionospheric disturbance is a very significant problem in remote sensing and navigation related applications. Dynamic ionospheric layers will witness variation of the plasmatic content which will results in generation of distorted radar images and often the most of the information captured by the image will be lost. The SAR images have vital applications in disaster monitoring, earth's surface monitoring, mapping of afforestation urbanizations hence the precision level required is higher. In the present study a fusion model of machine and deep learning approach is conducted a combination of GoogLeNet model with KNN, decision tree and SVM classifier is implemented for detection of Synthetic aperture radar image that is subjected to ionospheric variation. The results prove the detection of image affected by ionosphere can be detected put to 96 % and effective in implementing in real time. The data considered in the study is ALOSPALSAR data which is a L band radar data, the raw data is processed in a software called Envi SAR and the images as subjected to preliminary detection phase change method to check image is subjected to ionospheric and latter machine and deep learning approaches are considered**.**

Keywords— Synthetic Aperture Radar, Ionosphere, GoogLeNet

Introduction

The space-borne radar images especially synthetic aperture radar images are extensively used to military applications, mapping of soil moisture, afforestation, deforestation, urbanization, natural disasters such as floods, earthquakes, avalanche, volcanic deformation, melting of glaciers, vegetation cover and water body mapping. These SAR images are high resolution images and data is not lost during high cloud cover and capable of mapping in all-weather condition during day and night dynamic activities of earth's surface[1][2][3][4]. These images collect the information by restructuring the back scattered echoes from the earth's surface obtained coherently and processing simultaneously. The major roadblock for the efficient generation of error free images in dynamic ionospheric layer and low frequency signals are capable of generative images with highest detailing where as more prone to ionospheric disturbances and result in distorted images[5][6][7]. The dynamic variation of ionosphere is due to the dynamic change in the free electron content which varies due to change in sun's intensity, magnetic field of earth, variation at polar regions, seasonal and geographical variations. The sun spot number and solar cycle, solar maxima also responsible for variation of ionosphere which affects the SAR observations [8][9][10].

The ionosphere is frequently thought to be horizontally stratified and smooth at large sizes, but there are also many tiny scale abnormalities that resemble waves in the smooth background such as the electrojet, the aurora zone, the spread F layer, etc. The phenomenon known as ionospheric scintillation occurs when small-scale abnormalities significantly alter the character of radio waves. A mixture of free electrons, ions, and neutral gases

are produced in the ionosphere as a result of the ionisation of some air molecules by extremely powerful solar radiation [11][12][13]. The amount of free electrons in the atmosphere depends on the activity of the sun, the composition of the atmosphere, the location, the strength and direction of the Earth's magnetic field, and the time of day.

Methodology

The extensive survey was made to check the regions more prone to ionosphere disturbance in the earth and after the extensive survey Brazil amazon forest region the image captured on 26 March 2008 at 03:19:18 UT evidence of ionospheric streaking by ALOSPALSAR radar data. The free data for selected region of interest was available for ALOS PALSAR 1 satellite by JAXA space agency which is used in the study. The different set of data is used for both conditions that is during quiet and disturbed ionosphere condition for the same region of interest. Level 1.1 ALOSPALSAR data is used and initially is subjected to the first level processing in ENVI SAR software. The raw data is converted to image files that will be suitable for further processing[14][15][16]. The phase exchange module will initially check the preliminary detection of ionosphere effected image, after the initial confirmation of ionospheric disturbance, it is subjected to fusion approach of machine an deep learning using GoogLeNet with knn, svm and tree based classifier[17][18][19][20].

The methodology includes the data collection of the region of interest for both types of images with and without ionospheric disturbances of same region. The raw data is processed in ENVISAR software and preprocessed and labelled as without and with ionospheric disturbances and these data is trained to the fusion model of googLeNet with classifiers in further tested.

Figure 2: Methodology Schematic Diagram

Figure 3: The block diagram summaries the initial conversion of raw data to images JPEG format without losing the data in ENVI SAR software

The complete raw data folder is uploaded as input the data is resized based on the requirement the first level correction is implemented and geotag the coordinates as per the region of interest saved for required pixel format. The subset of the images is obtained based on the region of interest. The image with and without ionospheric effect is considered for the study. Both set of images are subjected to Fourier transformation and the

magnitude and phase component are separated and inverse Fourier transformation performed where the image with error phase is place for both images for reconstruction. The with and without images selected for the analysis are of same latitude, longitude. The phase of the image with disturbed ionospheric condition is placed for both set and any variation in the image phase can be compared with original image without ionospheric effects.

The GoogleNet model is the result of extensive research activity of Google which has reduction in the error rates for any type of analysis. It uses optimized techniques such as global average pooling and 1x1 convolutions in between the architecture model to improve the accuracy of the model. The 1x1 convolution usage will result is decreased number of weights and biases in the architecture which intern increase the architectural depth. GoogLeNet works with Global Average pooling at the terminating point of the network in which a feature map which is 7x7 is averaged into 1x1 which the reduce the number of training parameters to 0 and top-1 accuracy is increased by 0.6%. The inception module includes *1×1, 3×3, 5×5* convolution and combination of 3x3 max pooling is performed parallelly at input and output before the final output is generated and this enables the convolution filtering of different size to process the data at multiple scale. The intermediate brach of classifiers are used in the middle of the network architecture for training the data. These auxiliary classifiers include 5x5 average pooing and with three 1x1 stride that contains 128 filters along with two layers fully connected 1024 outputs and softmax classifier layer.

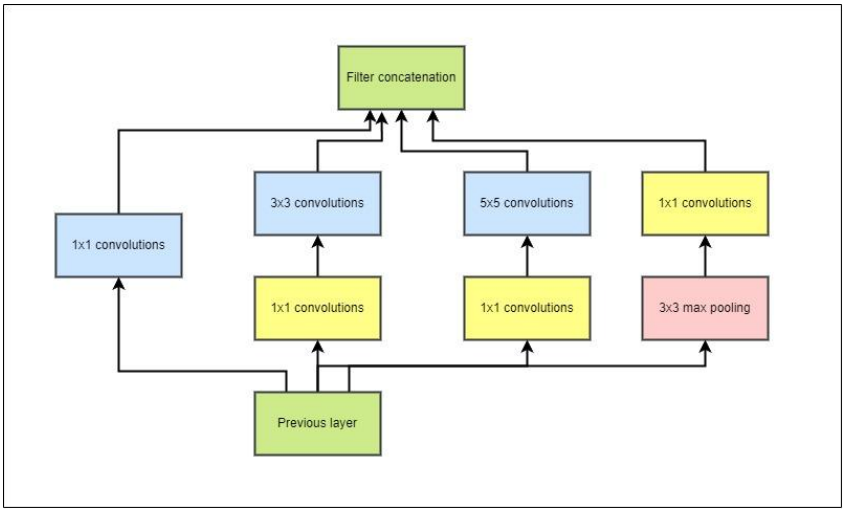

Figure 3: Model of interception with reduction in dimension in GoogLeNet

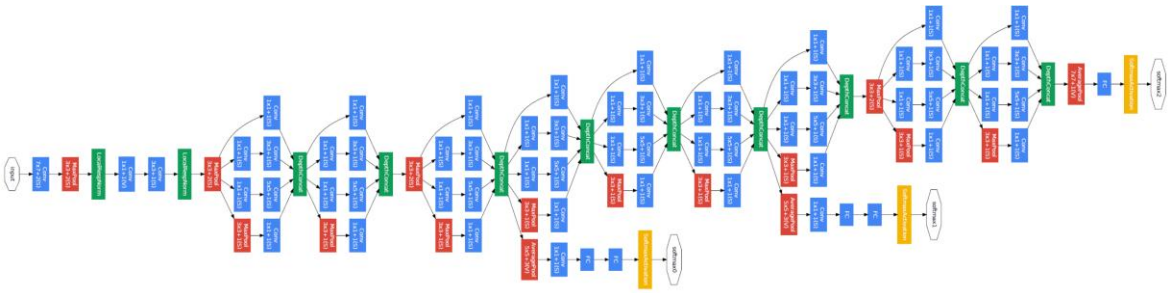

Figure 4: The architectural details of GoogLeNet

The KNN algorithm efficient non parametric algorithm with higher precision in classification an detection of different class of images. The higher feature dimension space is the disadvantage. The KNN is based on a learning method in which estimation and calculation of similarity of large samples, nonlinear classification time

in addition to this it will implement the training data processes faster and executes slow classification. The algorithm includes the K samples for the interpretation of the closest sample to be classified and chooses the classification category for the sample based on the K samples' category attributes. The distance between the training sample and the sample that needs to be categorised determines which K samples are the most comparable. The K value that is selected is crucial in the K-nearest neighbour classifier. The properties of the sample that needs to be categorised are not accurately reflected if the K value chosen is less. However, if the K value is chosen high, some samples that are not comparable to the samples that need to be classed are also included, which reduces the classification effect. Additionally, it has several drawbacks: KNN is a slow learning technique, caching all training samples before establishing a classification for the data. A big training set size or a high degree of dimensionality will result in a 0.8 reduction in classification accuracy. The conventional pixel-based categorization approach processes images at the pixel level. The categorization efficiency will be severely compromised by a big image area. Instead of using pixels to classify images, object-oriented image analysis utilises objects as primitives. The benefits of making full use of the colour, texture, shape, size, and context of ground objects are in addition to the fact that it can significantly reduce the amount of image processing data and increase classification accuracy.

SVM support vector they have been used extensively in satellite image categorization as well as machine vision domains like character, handwriting, digit, and text recognition SVMs have a reputation for being reliable, much like Artificial Neural Networks and other nonparametric classifiers. SVMs work by using a kernel function to nonlinearly project the training data in the input space to a feature space of higher (infinite) dimension. As a result, a linear classifier may distinguish between a dataset that is linearly separable. Remote sensing datasets, which are typically nonlinearly separable in the input space, can be categorised using this approach. In many cases, categorization in high dimension feature spaces causes the input space to be overfit.The decision tree algorithm is a member of the supervised learning algorithm family. The decision tree approach can be used to resolve classification and regression issues as well, unlike other supervised learning algorithms. A decision tree is used to learn simple decision rules that are inferred from training data in order to build a training model that can be used to predict the class or value of the target variable.

Results And Discussion

The results are evaluated for the real time data of the L band synthetic aperture radar L band data. The first stage results indicate the preliminary detection of the images affected by ionosphere. The complete image of the same region of interest is processed in ENVI SAR and the raw data is converted into small fragments which is considered as input to the fusion model of machine learning and deep learning The confusion matrix is a highly well-liked tool for resolving categorization issues. Both binary classification and multiclass classification issues can be solved with it. The counts from the predicted and actual values are represented by confusion matrices. The result "TN" stands for True Negative and displays the number of negatively classed cases that were correctly identified. Similar to this, "TP" stands for True Positive and denotes the quantity of correctly identified positive cases. The term "FP" denotes the number of real negative cases that were mistakenly categorized as positive, while "FN" denotes the number of real positive examples that were mistakenly classed as negative. Accuracy is one of the most frequently utilized metrics in classification. The formula below is used to determine a model's correctness (via a confusion matrix). Since accuracy might be deceptive when applied to unbalanced datasets, alternative metrics based on confusion matrix are also relevant for assessing performance. True Positive indicates the result predicted is correct and positive indicates validation. True negative indicates the predicted results are wrong or negative and that is true. The misclassification rate demonstrates how frequently your confusion matrix mis predicts the true positive and negative outputs. Add the false positive and false negative numbers together to get this result, then divide it by the total number of items in your data set. Prevalence indicates the total number of positive and true cases the results in the analysis is also calculated for different combination

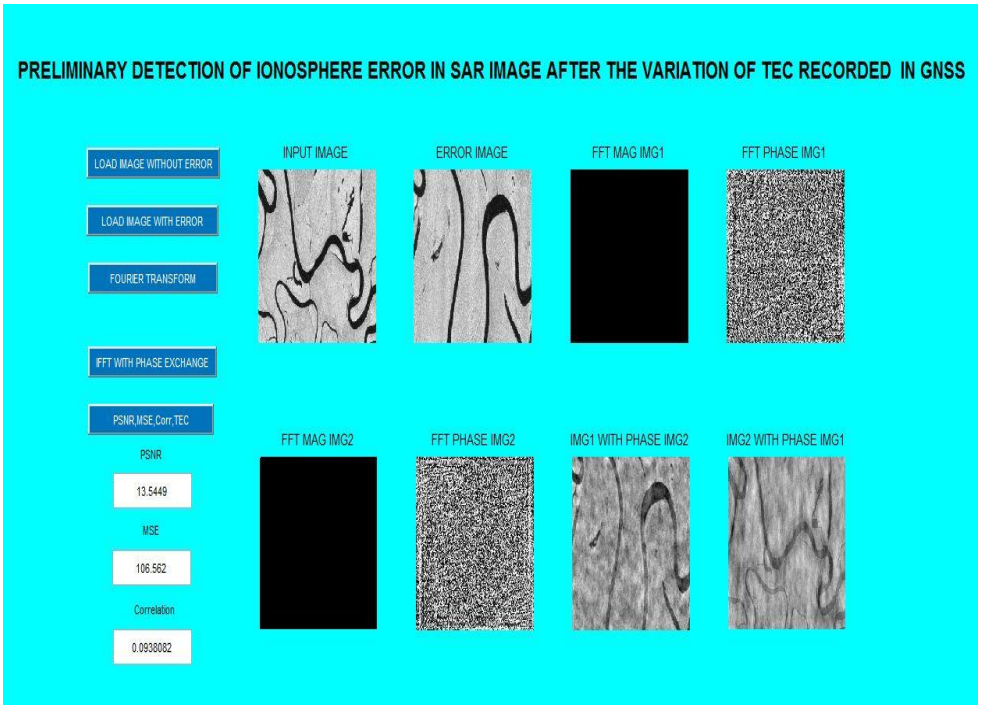

Figure 5: The above results indicate the analysis of phase change module when preliminary detection of ionospheric disturbance is verified. The two images with and without ionosphere disturbance.

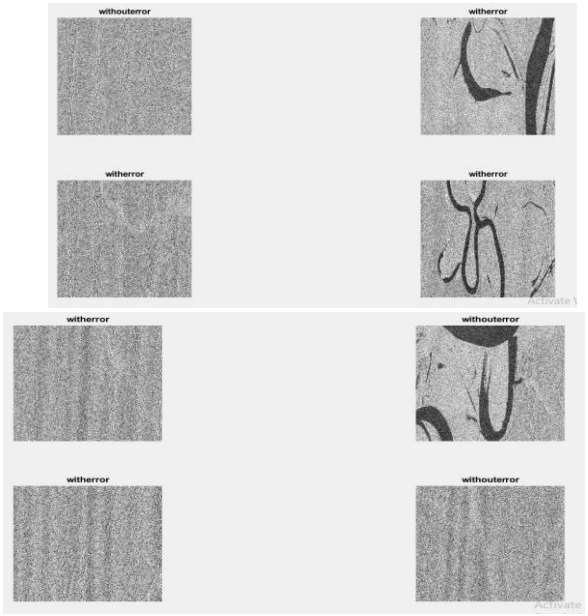

Figure 6: The above results indicate the with and without ionosphere disturbance selected for analysis.

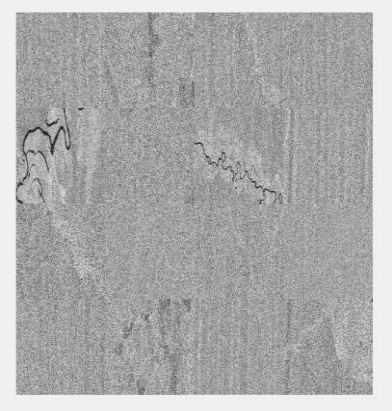

Figure 7a

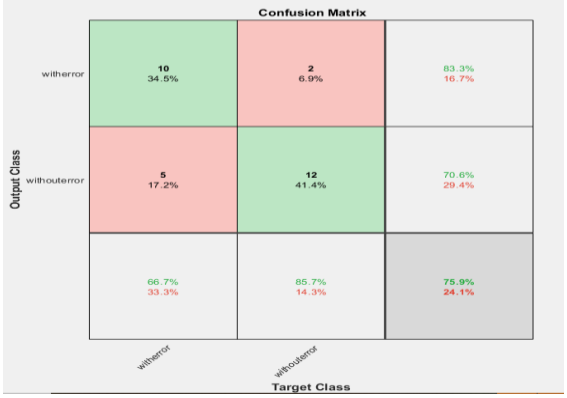

Figure 7b

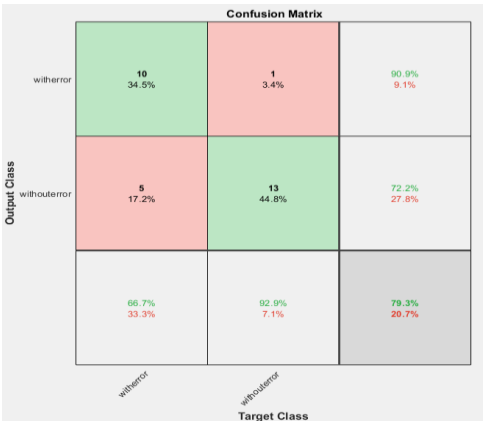

Figure 7c

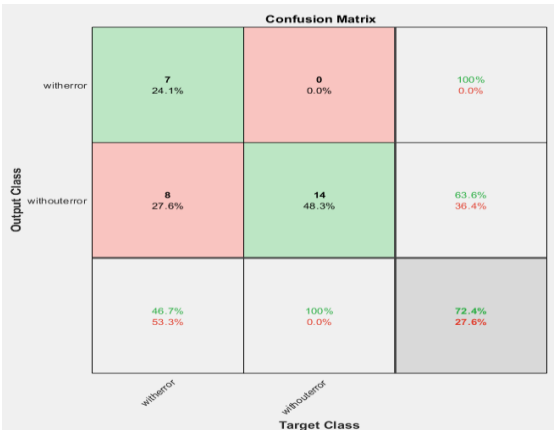

Figure 7d

Figure 7: a) The figure indicates the images selected for analysis. The other images indicate the confusion matrix obtained when GoogLeNet is interfaced with SVM, KNN and decision tree algorithms.

Table 1: results tabulated for the fusion model of GoogLeNet and SVM classifier algorithm is listed 90% training and 10% testing data.

	Accuracy	Misclassification	True negative	False positive	True negative	Precisio	Prevalence	F1_Score
1	0.8475	0.1525	0.8966	0.8667	0.8	0.8125	0.49	0.8525
2	0.8136	0.1864	0.8966	0.8667	0.7333	0.7647	0.49	0.8254
3	0.7797	0.2203	0.8276	0.8	0.7333	0.75	0.49	0.7869
4	0.7288	0.2712	0.7586	0.7333	0.7	0.7097	0.49	0.7333
5	0.7797	0.2203	0.7931	0.7667	0.7667	0.7667	0.49	0.7797
6	0.8136	0.1864	0.8621	0.8333	0.7667	0.7812	0.49	0.8197
7	0.7627	0.2712	0.2373	0.8276	0.8	0.7	0.73	0.4915
8	0.7288	0.23	0.8276	0.8	0.6333	0.6857	0.49	0.75
9	0.7966	0.2034	0.8276	0.8	0.7667	0.7742	0.49	0.8
10	0.78	0.28	0.845	0.8	0.66	0.77	0.5	0.8

Table 2: results tabulated for the fusion model of GoogLeNet and SVM classifier algorithm is listed 80% training and 20% testing data.

	Accuracy	Misclassificatio	True negative	False positive	True negative	precision	prevalence	F1_Score
1	0.8966	0.1034	0.8571	0.8	0.9333	0.9231	0.48	0.8889
2	0.9655	0.0345	1	0.9333	0.9333	0.9333	0.48	0.9655
3	0.8276	0.1724	0.7143	0.6667	0.9333	0.9091	0.48	0.8
4	0.8621	0.1379	0.9286	0.8667	0.8	0.8125	0.48	0.8667
5	0.8621	0.1379	0.8571	0.8	0.8667	0.8571	0.48	0.8571
6	0.8276	0.1724	1	0.9333	0.6667	0.7368	0.48	0.8485
7	0.7586	0.2414	0.7857	0.7333	0.7333	0.7333	0.48	0.7586
8	0.8966	0.1034	0.9286	0.8667	0.8667	0.8667	0.48	0.8966
9	0.8966	0.1034	0.9286	0.8667	0.8667	0.8667	0.48	0.8966
10	0.7241	0.2759	0.8571	0.8	0.6	0.6667	0.48	0.75

	Accuracy	Misclassification	True negative	False positive	True negative	Precision	Prevalence	F1_Score
1	91.53%	0.0847	0.931	0.9	0.9	0.9	0.49	0.9153
2	0.8983	0.1017	0.8276	0.8	0.9667	0.96	0.49	0.8889
3	0.9153	0.0847	0.931	0.9	0.9	0.9	0.49	0.9153
4	0.8305	0.1695	0.7931	0.7667	0.8667	0.8519	0.49	0.8214
5	0.8983	0.1017	0.8276	0.8	0.9667	0.96	0.49	0.8889
6	0.8305	0.1695	0.7931	0.7667	0.8667	0.8519	0.49	0.8214
7	0.8644	0.1356	0.8276	0.8	0.9	0.8889	0.49	0.8571
8	0.8136	0.1864	0.8621	0.8333	0.7667	0.7812	0.49	0.8197
9	0.7966	0.2034	0.8276	0.8	0.7667	0.7742	0.49	0.81
10	0.8475	0.1525	0.8276	0.8	0.8667	0.8571	0.49	0.8421

Table 3: results tabulated for the fusion model of GoogLeNet and KNN classifier algorithm is listed 80% training and 20% testing data.

	Accuracy	Misclassification	True position	False positive	True negative	Precision	Prevalence	F1_Score
1	89.66%	0.1034	0.9286	0.8667	0.8667	0.8667	0.48	0.8966
2	0.8966	0.1034	0.8571	0.8	0.9333	0.9231	0.48	0.8889
3	0.8966	0.1034	0.7857	0.7333	1	1	0.48	0.88
4	0.8621	0.1379	0.8571	0.8	0.8667	0.8571	0.48	0.8571
5	0.9655	0.0345	0.9286	0.8667	1	1	0.48	0.963
6	0.9655	0.0345	1	0.9333	0.9333	0.9333	0.48	0.9655
7	0.8621	0.1379	0.9286	0.8667	0.8	0.8125	0.48	0.8667
8	0.7586	0.2414	0.8571	0.8	0.6667	0.7059	0.48	0.7742
9	0.8621	0.1379	0.8571	0.8	0.8667	0.8571	0.48	0.8571
10	0.8966	0.1034	0.9286	0.8667	0.8667	0.8667	0.48	0.8966

Table 4: results tabulated for the fusion model of GoogLeNet and KNN classifier algorithm is listed 90% training and 10% testing data.

	Accuracy	Misclassification	True position	False positive	True negative	Precision	Prevalence	F1_Score
1	81.36%	0.1864	0.8276	0.8	0.8	0.8	0.49	0.8136
2	0.7966	0.2034	0.7586	0.7333	0.8333	0.8148	0.49	0.7857
3	0.8136	0.1864	0.8966	0.8667	0.7333	0.7647	0.49	0.8254
4	0.7458	0.2542	0.6897	0.6667	0.8	0.7692	0.49	0.7273
5	0.7966	0.2034	0.7931	0.7667	0.7931	0.8	0.49	0.7931
6	0.7288	0.2712	0.6897	0.6667	0.7667	0.7407	0.49	0.7143
7	0.7797	0.2203	0.7931	0.7667	0.7667	0.7667	0.49	0.4915
8	0.7458	0.2542	0.8276	0.8	0.6667	0.7059	0.49	0.7619
9	0.7119	0.2881	0.7241	0.7	0.7	0.7059	0.49	0.7119
10	0.7458	0.2542	0.7586	0.7333	0.7333	0.7333	0.49	0.7458

.

Table 4: results tabulated for the fusion model of GoogLeNet and decision tree classifier algorithm is listed 80% training and 20% testing data.

	Accuracy	Misclassificati	True position	False positive	True negative	Precision	Prevalence	F1_Score
1	86.21%	0.1379	0.7143	0.6667	1	1	0.48	0.8333
2	0.6897	0.3103	0.8571	0.8	0.5333	0.6316	0.48	0.7273
3	0.7931	0.2069	0.7857	0.7333	0.8	0.7857	0.48	0.7857
4	0.7931	0.2069	0.7857	0.7333	0.8	0.7857	0.48	0.7857
5	0.7931	0.2069	0.7857	0.7333	0.8	0.7857	0.48	0.7857
6	0.7241	0.2759	0.6429	0.6	0.8	0.75	0.48	0.6923
7	0.7586	0.2414	0.7857	0.7333	0.7333	0.7333	0.48	0.7586
8	0.7931	0.2069	0.7857	0.7333	0.8	0.7857	0.48	0.7857
9	0.80	0.2759	0.8571	0.8	0.6	0.6667	0.48	0.75

Table 4: results tabulated for the fusion model of GoogLeNet and KNN classifier algorithm is listed 90% training and 10% testing data.

Conclusion

The machine learning and deep learning fusion model used for detection of with and without ionospheric effects is efficiently working up to an accuracy level of 96.554% the results show that the state vector machine and googLenet combination works better and next possible combination is GoogLeNet with KNN and GoogLenet and decision tree-based model will be last priority. The analysis completed for all combination of training and testing data set. The results are evaluated for different parameters using real time synthetic aperture radar L band ALOSPALSAR. The parameters like misclassification, true negative, false positive, precision and prevalence and F1 scores are obtained for all three combination of fusion model the results are comparatively good for SVM along with GoogleNet. The study can be further extended using different classifiers and network models for the same dataset and can be tested can accuracy be achieved more than 96.554%.

Acknowledgments

The data used in the study is free data available in the ALOSPALSAR Alaska data-based authors are thankful to Alaska Satellite Facility. The raw data of ALOSPALSAR 1 satellite is available for the region of interest is useful for the conduction of studies related to ionosphere.

References

[1] Zhang, L.; Zhang, L. Artificial Intelligence for Remote Sensing Data Analysis: A review of challenges and opportunities. *IEEE Geosci. Remote Sens. Mag.* **2022**, *10*, 270–294.

[2] Xu, X.; Zhang, X.; Zhang, T. Lite-YOLOv5: A Lightweight Deep Learning Detector for On-Board Ship Detection in Large-Scene Sentinel-1 SAR Images. *Remote Sens.* **2022**,

[3] Kačan, M.; Turčinović, F.; Bojanjac, D.; Bosiljevac, M. Deep Learning Approach for Object Classification on Raw and Reconstructed GBSAR Data. *Remote Sens.* **2022**,

[4] Aa, E., Zhang, S.-R., Wang, W., Erickson, P. J., Qian, L., Eastes, R., et al. (2022). Pronounced Suppression and X-Pattern Merging of Equatorial Ionization Anomalies After the 2022 Tonga Volcano Eruption. *Journal of Geophysical Research: Space Physics*, **127**(6), e2022JA030527. https://doi.org/10.1029/2022JA030527

[5] Aa, E., Zou, S., Eastes, R., Karan, D. K., Zhang, S.-R., Erickson, P. J., & Coster, A. J. (2020). Coordinated ground-based and space-based observations of equatorial plasma bubbles. *Journal of Geophysical Research: Space Physics*, **125**(1), e27569. https://doi.org/10.1029/2019JA027569

[6] Aa, E., Zhang, S.-R., Erickson, P. J., Coster, A. J., Goncharenko, L. P., Varney, R. H., & Eastes, R. (2021). Salient Midlatitude Ionosphere-Thermosphere Disturbances Associated With SAPS During a Minor but Geo-Effective Storm at Deep Solar Minimum. *Journal of Geophysical Research: Space Physics*, **126**(7), e29509. https://doi.org/10.1029/2021JA029509

[7] Detecting the deformation anomalies induced by underground construction using multiplatform MT-InSAR: a case study in to Kwa wan Station, Hong Kong IEEE J. Sel. Top. Appl. Earth Obs., 14 (2021), pp. 9803-9814, 10.1109/JSTARS.2021.3113672

[8] Aa, E., Zou, S., Eastes, R., Karan, D. K., Zhang, S.-R., Erickson, P. J., & Coster, A. J. (2020). Coordinated ground-based and space-based observations of equatorial plasma bubbles. *Journal of Geophysical Research: Space Physics*, **125**(1), e27569. https://doi.org/10.1029/2019JA027569

[9] Aa, E., Zou, S., & Liu, S. (2020). Statistical analysis of equatorial plasma irregularities retrieved from Swarm 2013–2019 observations. *Journal of Geophysical Research: Space Physics*, **125**(4), e27022. https://doi.org/10.1029/2019JA027022

[10] Aa, E., Zou, S., Eastes, R., Karan, D. K., Zhang, S.-R., Erickson, P. J., & Coster, A. J. (2020). Coordinated ground-based and space-based observations of equatorial plasma bubbles. *Journal of Geophysical Research: Space Physics*, **125**(1), e27569. https://doi.org/10.1029/2019JA027569

[11] Aa, E., Zhang, S.-R., Erickson, P. J., Coster, A. J., Goncharenko, L. P., Varney, R. H., & Eastes, R. (2021). Salient Midlatitude Ionosphere-Thermosphere Disturbances Associated With SAPS During a Minor but Geo-Effective Storm at Deep Solar Minimum. *Journal of Geophysical Research: Space Physics*, **126**(7), e29509. https://doi.org/10.1029/2021JA029509

[12] Franz J. Meyer,"Performance Requirements for Ionospheric Correction of Low-Frequency SAR Data," IEEE Geoscience and remote sensing, vol. 49, no. 10 pp. 3694–3702, 2011.

[13] Christopher R. Mannix, David P. Belcher, and Paul S. Cannon, "Measurement of Ionospheric Scintillation Parameters From SAR Images Using Corner Reflectors," IEEE Geoscience and remote sensing, vol. 55, no. 12, pp. 6695–6702, 2017.

[14] Elvira Music` o , Claudio Cesaroni, Luca Spogli, John Peter Merryman Boncori, Giorgiana De Franceschi, and Roberto Seu, "The Total Electron Content From InSAR and GNSS: A Midlatitude Study," IEEE journal of selected topics in applied earth observations and remote sensing, vol. 11, no. 5 pp. 237–239, 2018.

[15] Zhuoqun Wang, Yajun Li, Yong Huang, Yanbin Li "CS Imaging Method for Geosynchronous SAR considering to Ionospheric Effects," *J. Syst. Eng. Electron.*, vol. 27, no. 5, pp. 993–1000, 2016.

[16] Cheng Wang, Liang Chen, and Lu Liu,"Analysis of Computerized Ionospheric Tomography Using PALSAR Polarimetric Data,"IEEE vol. 54, no. 3, pp. 1446–1461, 2016.

[17] J. Liu, Y. Kuga, A. Ishimaru, X. Pi, and A. Freeman, "Measurement of Ionospheric Faraday Rotation in Simulated and Real Spaceborne SAR Dat," *IEEE Trans. Geosci. Remote Sens.*, vol. 71, no. 5 PART 1, pp. 1512–9, .

[18] Michael Jehle, David Small, "Measurement of Ionospheric TEC in Spaceborne SAR Data," vol. 48, no. 6, pp. 1842–1844, 1999.

[19] Christopher R. Mannix1, David P. Belcher1, Paul S. Cannon1, and Matthew J. Angling "Using GNSS signals as a proxy for SAR signals: Correcting ionospheric defocusing," American Geophysical Union.48, no. 06, pp. 60–70, 2015.

[20] Zehra cammlica, H.R Tizhoosh and Farzad Khalvati, "Medical Image Classification via SVM using LBP Features from Saliency-Basd Folded Data", International conference on Machine Learning and Applications, IEEE, 2015.